Extended Data

Type III CRISPR-Cas complexes act as protein-assisted ribozymes during target RNA cleavage

Evan A. Schwartz, Jack P.K. Bravo, Mohd Ahsan, Luis A. Macias, Caitlyn L. McCafferty, Tyler L. Dangerfield, Jada N. Walker, Jennifer S. Brodbelt, Giulia Palermo, Peter C. Fineran, Robert D. Fagerlund, and David W. Taylor

Extended Data Table 1 | Theoretical masses, experimental masses, and % deviation of the type III-Dv complex, subcomplexes, and individual subunits. Experimental masses were recorded via native and LC-mass spectrometry.

Type III-Dv Complex	Theoretical mass (Da)	Native MS Experimental mass (Da)	Denaturing LC-MS Experimental mass (Da)	Deviation from expected mass (%)*
Cas7_insert•Cas7-Cas5-Cas11•Cas10-His6•Cas7-2x•Csx19•mature crRNA	331,405	332,300	-	0.27
Cas7_insert•Cas7-Cas5-Cas11•Cas10-His6•Cas7-2x•mature crRNA	310,213	310,980	-	0.25
Cas7_insert•Cas7-Cas5-Cas11•Cas10-His6•Csx19•mature crRNA	274,778	274,840	-	0.02
Cas7_insert•Cas7-Cas5-Cas11•Cas7-2x•Csx19•mature crRNA	267,286	267,770	-	0.18
Cas10-His6•mature crRNA	76,055	-	76,110	0.07
Cas7_insert	90,080	-	90,080	0.00
Cas7-Cas5-Cas11	87,451	-	87,450	0.00
Cas10-His6	64,119	64,170	64,120	0.00
Cas7-2x	56,627	-	56,630	0.01
Csx19	21,192	21,190	21,190	0.01
Mature crRNA	11,936	-	-	-

Extended Data Table 2 | Model Statistics for the type III-Dv binary complex, non-self target-bound complex, and self target pre-cleavage and post-cleavage complexes.

	Binary Complex	Non-Self Target-Bound Complex	Self Target Pre-Cleavage Complex	Self Target Post-cleavage complex
Data collection and processing	cryoSPARC v2	cryoSPARC v2	cryoSPARC v3	cryoSPARC v3
Magnification	105,000x	105,000x	105,000x	105,000x
Voltage (kV)	300	300	300	300
Electron exposure (e–/Å^2)	80.5	80.5	80	80
Defocus range (μm)	1.2-2.2	1.2-2.2	1.2-2.2	1.2-2.2
Pixel size (Å)	0.81	0.81	0.8332	0.8332
Symmetry imposed	C1	C1	C1	C1
Initial particle images (no.)	1,890,840	1,919,796	1,280,364	1,280,364
Final particle images (no.)	648,782	609,722	181,656	41,202
Map resolution (Å) FSC threshold	2.5 0.143	2.8 0.143	3.0 0.143	3.4 0.143
Map resolution range (Å)	N/A	N/A	N/A	N/A
Refinement				
Model resolution (Å) FSC threshold	2.6 0.5	2.8 0.5	3.1 0.5	3.7 0.5
Model resolution range (Å)	N/A	N/A	N/A	N/A
Map sharpening *B* factor (Å^2)	99.3	124.7	114.1	97.5
Model composition Non-hydrogen atoms Protein residues Ligands	 21968 2692 0	 22598 2685 0	 22589 2685 0	 22405 2697 0
B factors (Å^2) Protein Nucleotide	 14.56/101.45/47.39 15.79/67.58/30.46	 15.07/97.79/50.92 16.14/80.16/36.66	 13.69/81.92/40.10 12.49/79.61/28.83	 46.76/162.27/88.37 54.04/126.03/72.68
R.m.s. deviations Bond lengths (Å) Bond angles (°)	 0.008 0.894	 0.007 0.866	 0.005 0.786	 0.006 0.801
Validation MolProbity score Clashscore Poor rotamers (%)	 1.65 4.54 1.85	 1.66 5.19 1.37	 1.50 2.10 2.08	 1.59 3.15 1.76
Ramachandran plot Favored (%) Allowed (%) Disallowed (%)	 96.60 3.18 0.22	 95.91 3.79 0.30	 96.02 3.71 0.26	 95.71 3.88 0.41

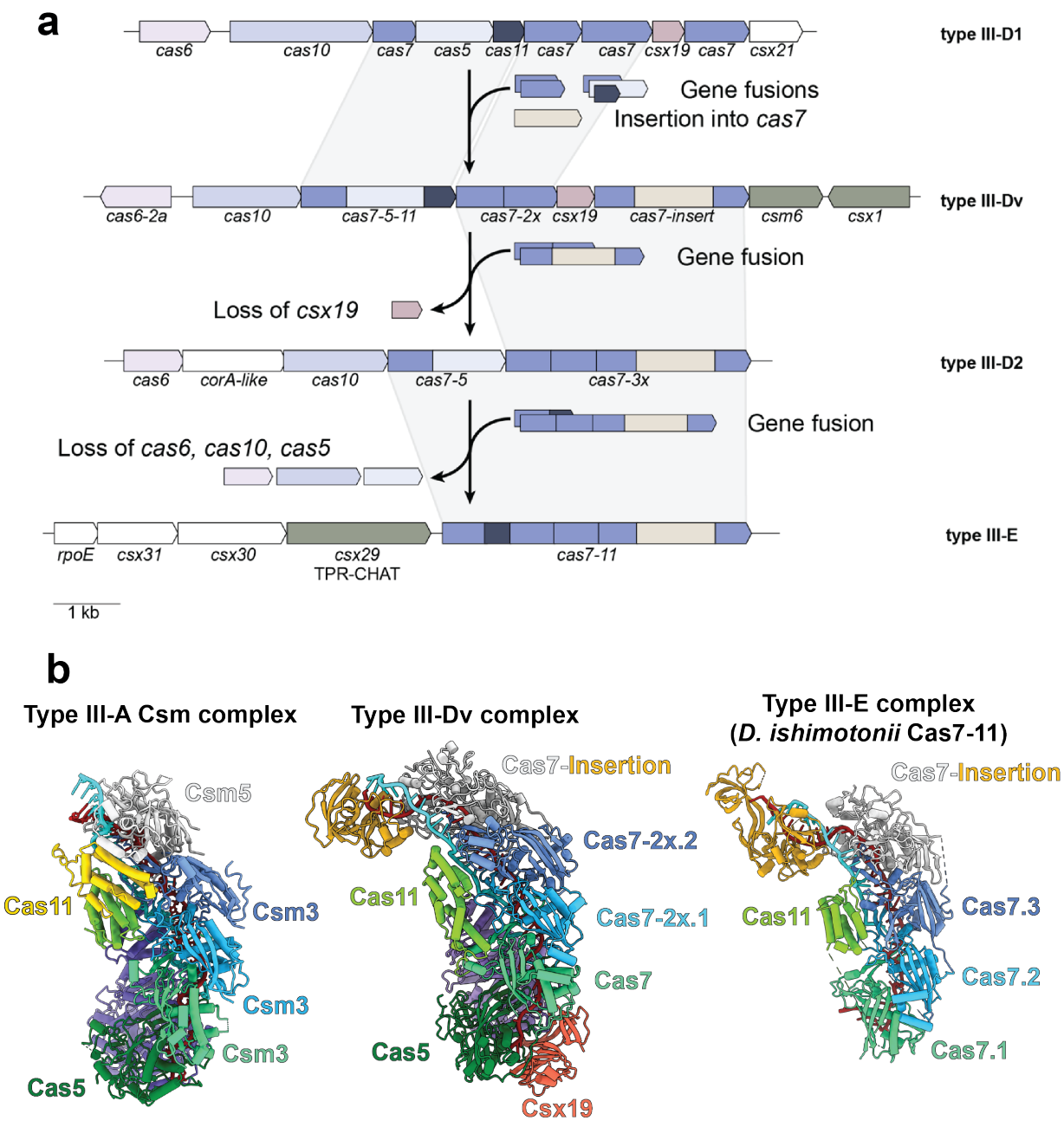

Extended Data Fig. 1 | Proposed evolution of type III CRISPR-Cas systems. a, Putative evolutionary progression from type III-D1 to type III-E, with other multi-subunit type III systems presumably preceding type III-D1. **b,** Structural comparison between the multi-subunit type III-A (Csm) complex (PDB: 6IFY), the multi-subunit type III-Dv complex containing many subunit fusions, and the single-subunit type III-E complex (PDB: 7WAH).

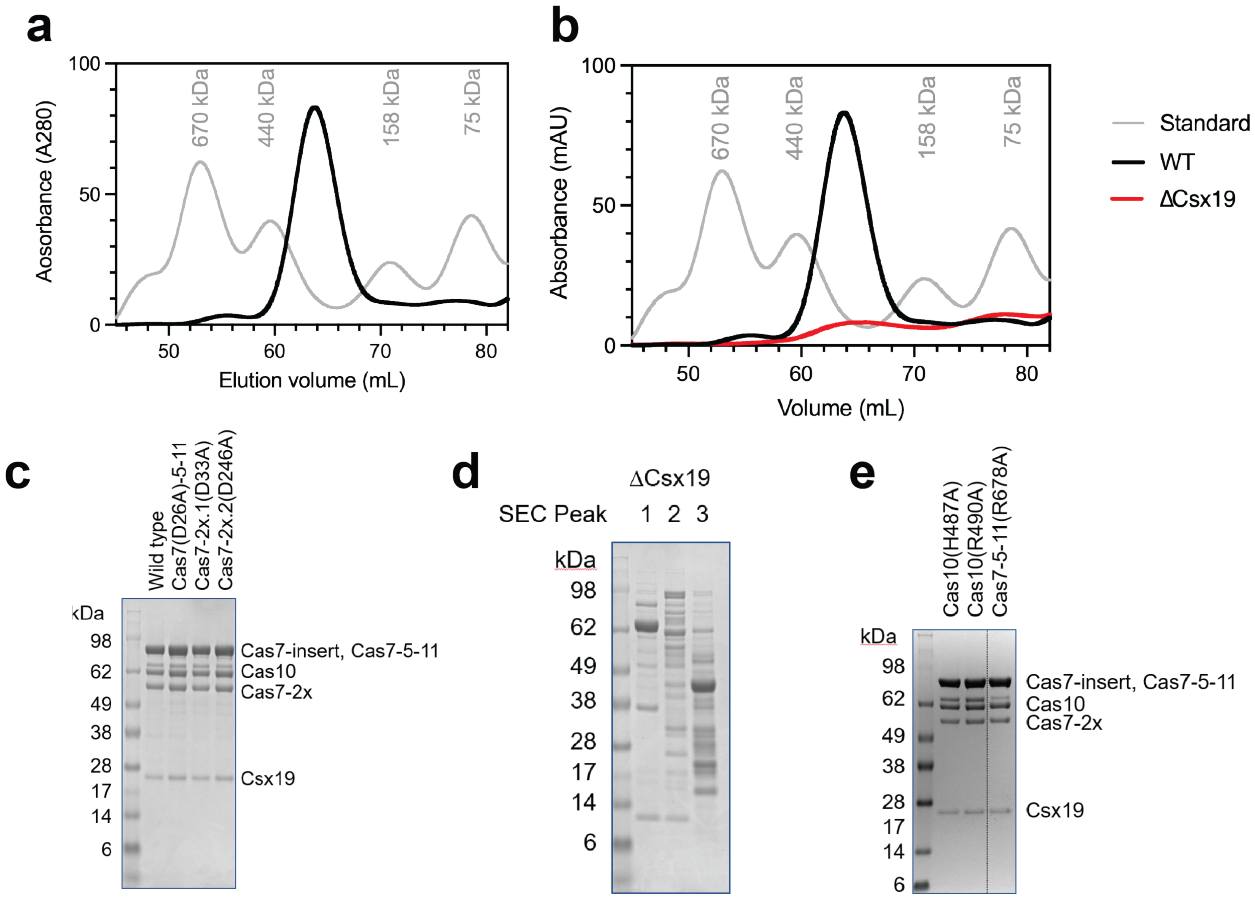

Extended Data Fig. 2 | Purification of the type III-Dv effector complex. a, Size-exclusion chromatograph of the WT type III-Dv complex. Black peak corresponds to ~330 kDa. Grey peaks represent standardized molecular weights. **b,** Size-exclusion chromatograph of the ΔCsx19 type III-Dv complex purification (red trace). Black peak corresponds to wild-type III-Dv complex. Grey peaks represent standardized molecular weights. **c,** Purification of Cas7 active site aspartate mutants for RNA cleavage analysis. **d,** SDS-PAGE of the ΔCsx19 from the two broad peaks seen in **b**. No complex appeared to form. **e,** Purification of other Cas7 active site residues predicted to be involved in RNA cleavage acid-base catalysis.

a Binary

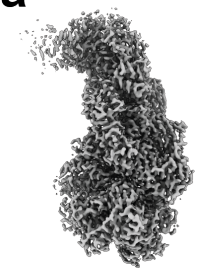

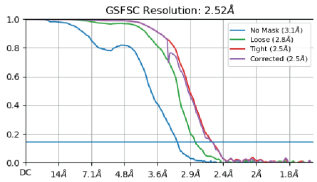

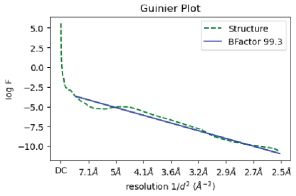

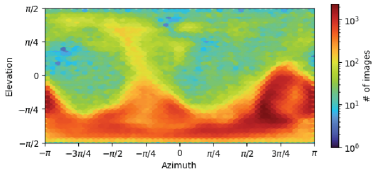

Binary Local Refinement

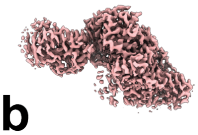

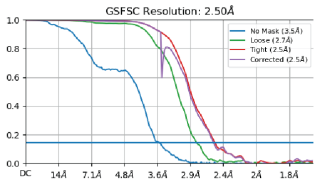

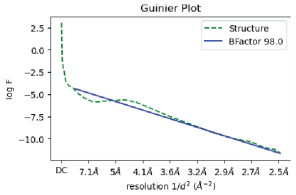

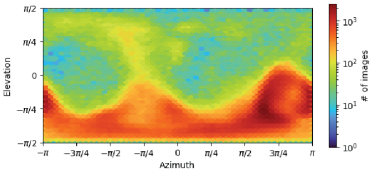

b Non-self target-bound

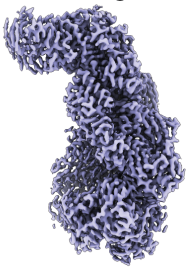

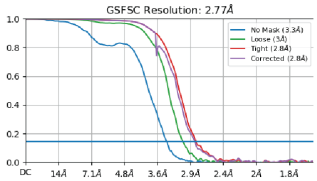

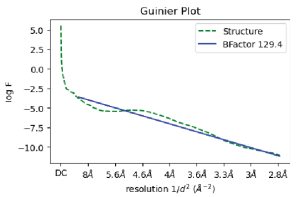

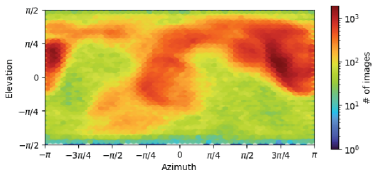

Non-self Local Refinement

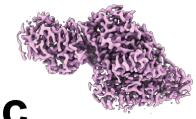

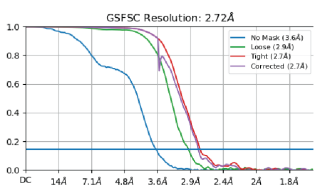

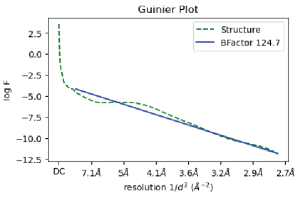

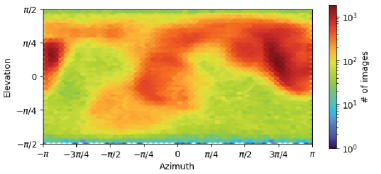

c Self target, Mg^{2+}-bound

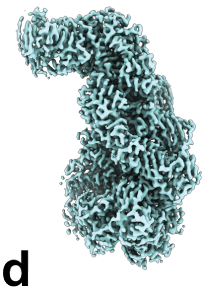

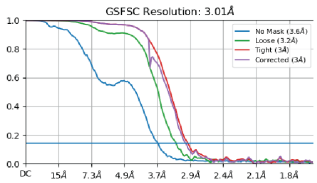

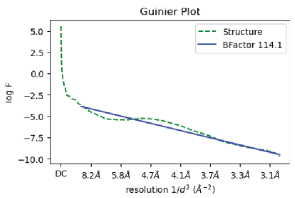

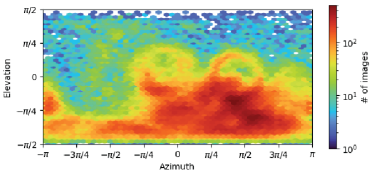

d Post-cleavage

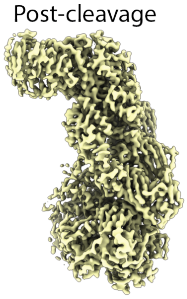

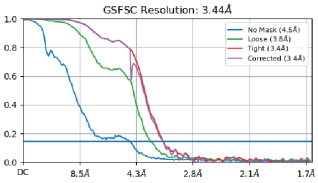

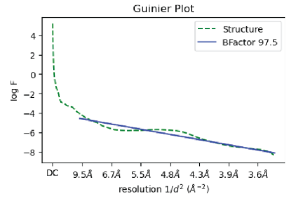

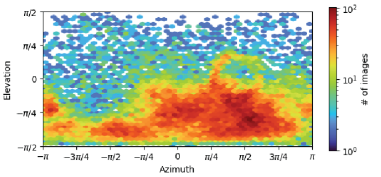

Extended Data Fig. 3 | EM validation of type III-Dv maps. Final reconstructions, FSC plots for resolution determination, Guinier plot for b-factor sharpening, and directional distribution plots of the type III-Dv **a,** binary consensus (top) and local refinement (bottom) structures **b,** non-self target-bound consensus and local refinement structures **c,** Self target and Mg^{2+}-bound structure and **d,** Self target-bound post-cleavage structure.

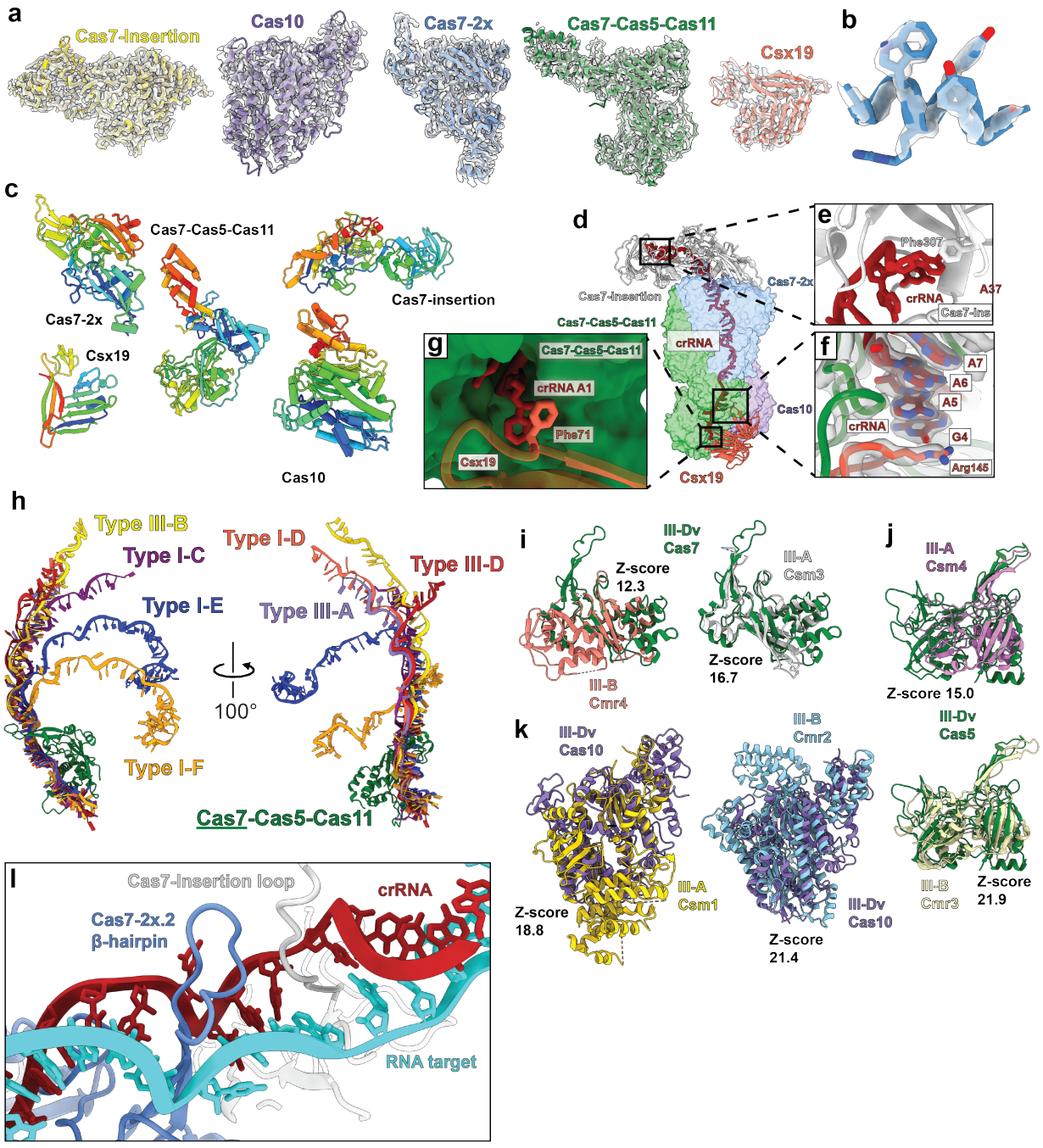

Extended Data Fig. 4 | Analysis of type III-Dv subunits, crRNA, and RNA target. a, Individual subunits fit into their respective cryo-EM density. **b,** Density of an alpha-helix in the Cas7-insertion subunit. **c,** Connectivity of the type III-Dv subunit structures. The subunits are colored N-terminus (blue) to C-terminus (red). **d,** crRNA trajectory through the type III-Dv effector complex. **e,** 3' crRNA capping by Phe307 of Cas7-insertion. **f,** 5' crRNA capping by Phe71 of Csx19. **g,** Arg145 of Csx19 interacting with G4 of the crRNA, upstream of the 5' crRNA handle. **h,** crRNA geometry comparison between type III-Dv and other type I and type III systems. **i,** Structural alignments between the III-Dv Cas7 domain of Cas7-Cas5-Cas11 with Cmr4 (Cas7) of the type III-B (peach, Z-score 12.3) and Csm3 of the type III-A complex (white, Z-score 16.7); **j,** III-Dv Cas5 domain of Cas7-Cas5-Cas11 with Cas5 (Csm4) of the type III-A complex (magenta, Z-score 15.0) and Cas5

(Cmr3) of the type III-B complex (beige, Z-score 21.9); **k,** III-Dv Cas10 subunit with Cas10 (Csm1) of the type III-A complex (yellow) and Cas10 (Cmr2) of the type III-B complex (cyan). **l,** Comparison between the protrusion of the Cas7-2x.2 beta-hairpin and Cas7-insertion loop between the crRNA and the RNA target duplex.

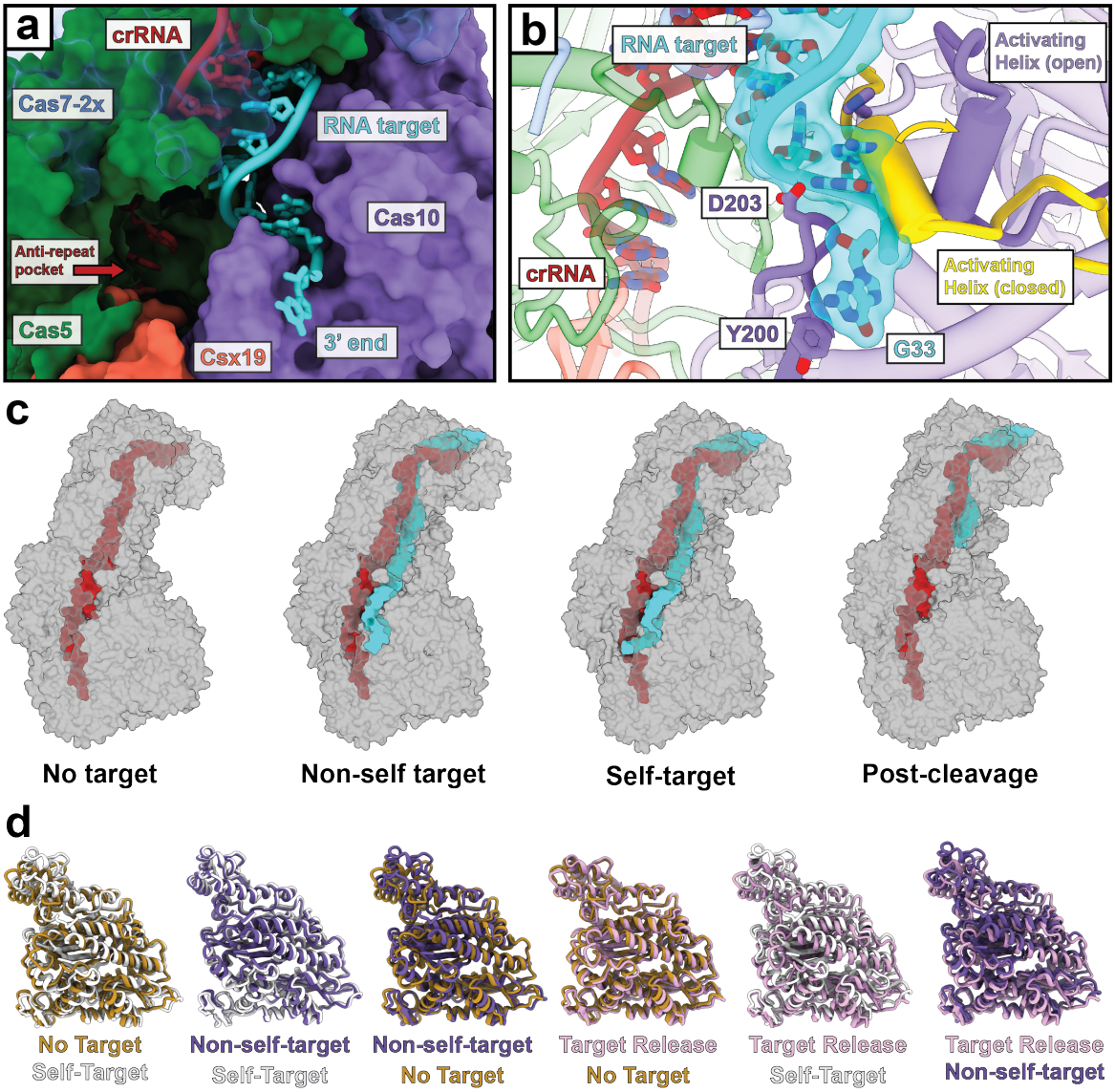

Extended Data Fig. 5 | Cas10 activation by non-self RNA binding. a, Path of the RNA target strand gets directed through Cas10 rather than into the anti-repeat pocket. **b,** Upon binding a non-self RNA target, an activating helix in Cas10 gets pushed by the target RNA into an active conformation. Yellow arrow indicates directionality of movement of this alpha helix. **c,** Structures of the type III-Dv complex before target binding, after non-self- and self-target binding, and in a post-cleavage state. **d,** Conformational changes within Cas10 between the different structures described in **c.**

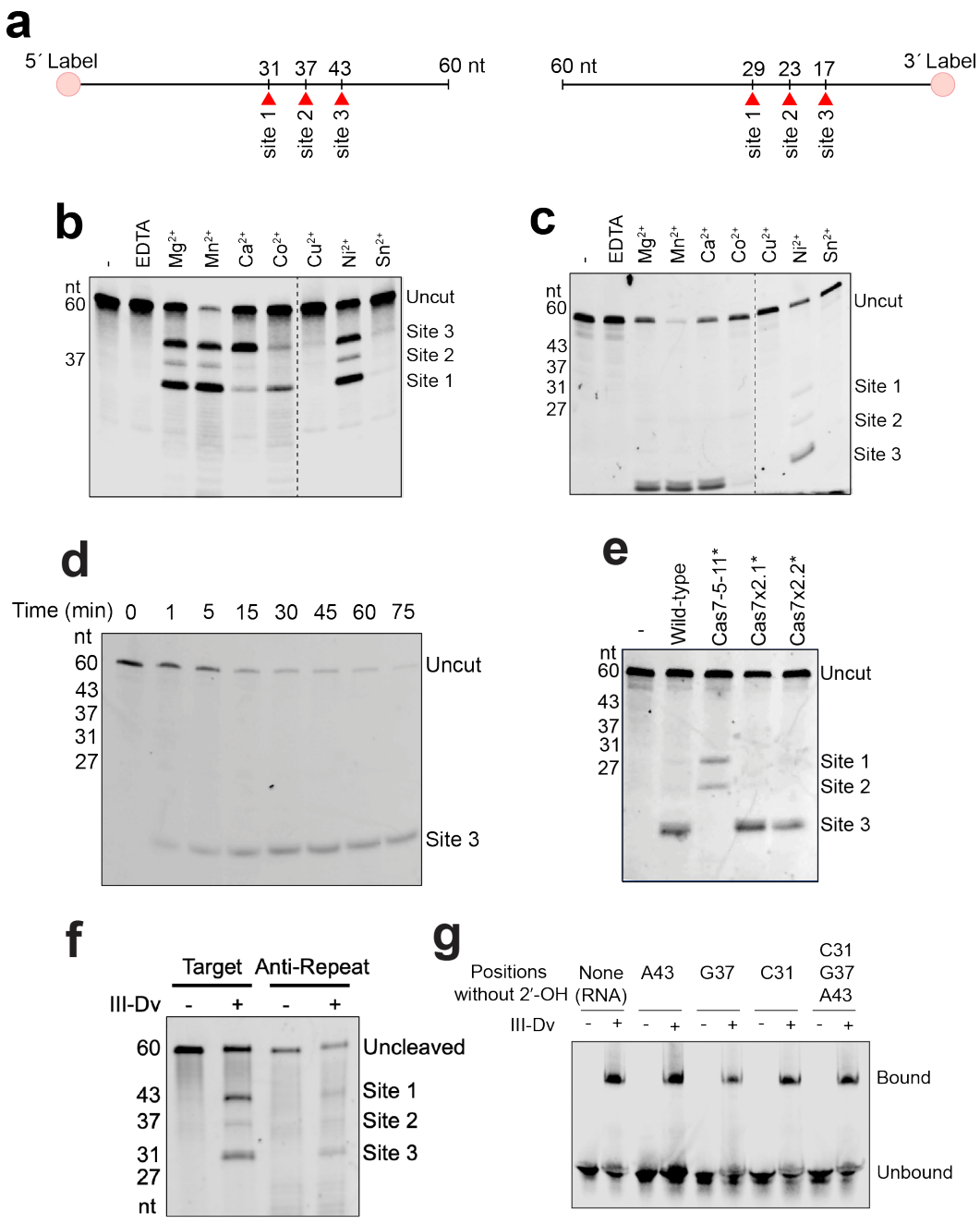

Extended Data Fig. 6 | Electrophoretic Mobility Shift Assays of RNA target cleavage and binding type III-Dv. a, Fluorescent probes used in RNA cleavage reactions. **b,** Metal dependent cleavage of the 5'-labelled RNA target. Cleavage site 1, 2, and 3 correspond to 31, 37, and 43 nucleotide products, respectively. **c,** Metal dependent cleavage of the 3'-labeled RNA target. Cleavage site 1, 2, and 3 correspond to 29, 23, and 17 nucleotide products, respectively. **d,** RNA cleavage time course with a 3'-labeled RNA target across 75 minutes. **e,** 3'-labeled RNA cleavage analysis after mutagenesis of the three active site residues of Cas7-Cas5-Cas11, Cas7-2x.1, and Cas7-2x.2. **f,** Comparison of RNA cleavage of Non-Self RNA target (left) and Self RNA target (right). **g,** Binding of a DNA-RNA hybrid target by the type III-Dv complex with 2'-OH groups removed at specified positions.

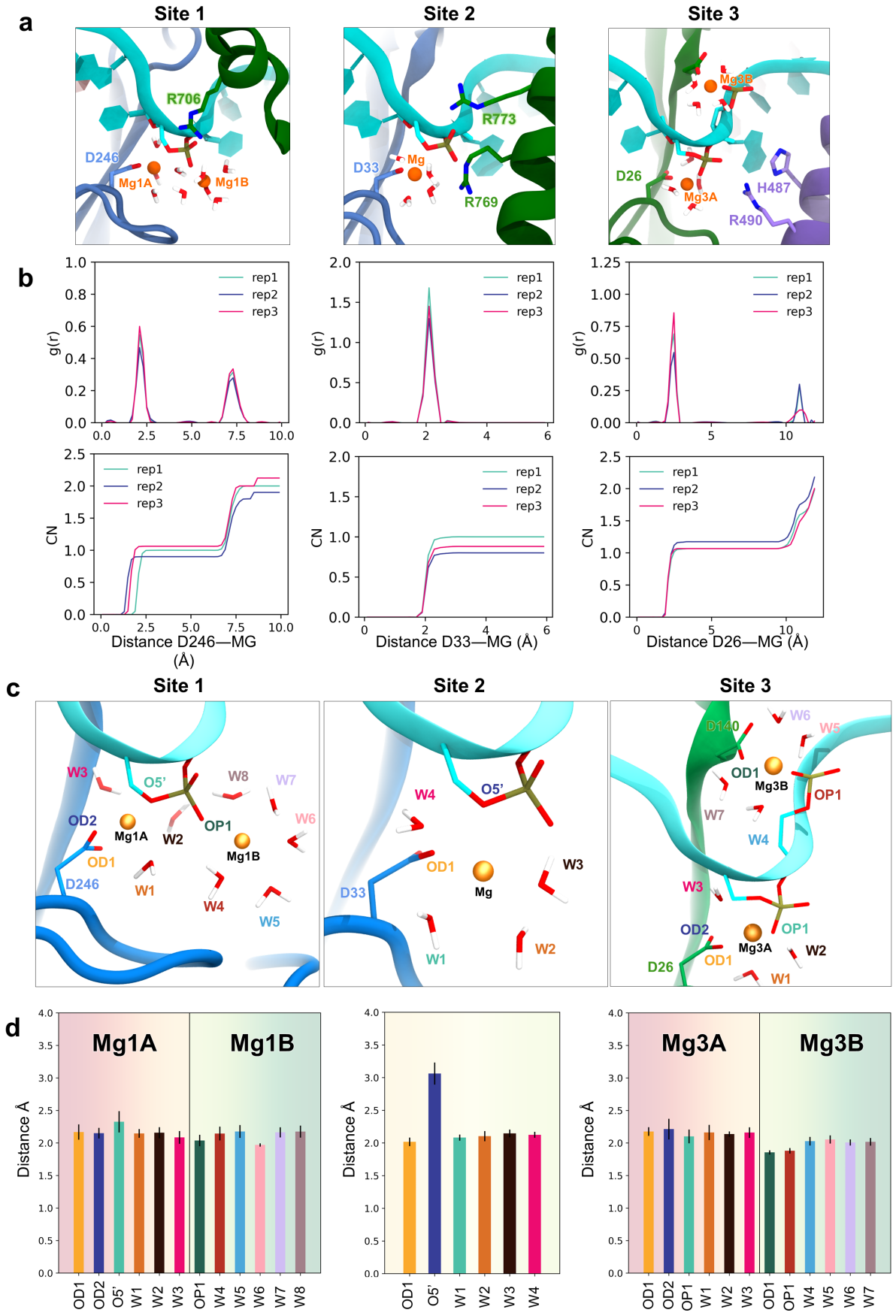
a
Site 1
Site 2
Site 3
R706
D246
Mg1A
Mg1B
R773
D33
Mg
R769
Mg3B
D26
Mg3A
H487
R490
b
rep1
rep2
rep3
g(r)
CN
Distance D246—MG (Å)
Distance D33—MG (Å)
Distance D26—MG (Å)
c
Site 1
Site 2
Site 3
W3
O5'
W8
W7
W6
OD2
Mg1A
W2
OP1
Mg1B
OD1
D246
W1
W4
W5
D33
Mg
D140
OD1
Mg3B
OP1
W7
W4
OD2
Mg3A
D26
d
Mg1A
Mg1B
Mg3A
Mg3B
Distance Å
OD1
OD2
O5'
W1
W2
W3
OP1
W4
W5
W6
W7
W8

Extended Data Fig. 7 | Analysis of the three active sites of the type III-Dv complex. a, Representative snapshot showing the placement of Mg^{2+} ion at each active site of type III-Dv CRISPR-Cas effector complex during μs-long MD simulation. **b,** Radial distribution function g(r) and coordination number calculated obtained from the all-atom MD simulation shows sites 1 and 3 can accommodate two Mg^{2+} ions while site 2 takes in only one Mg^{2+} ion. These results were consistent in all three replicas. **c,** The coordination of the metal ions attained during ~40 ps of ab-initio QM(Car-Parrinello)/MM MD is shown for the three active sites. **d,** Distances between the Mg^{2+} ion and key atoms involved in its coordination is shown for each catalytic site, distance is the average of stable last ~20 ps of QM/MM simulation and error bars represent standard deviation.

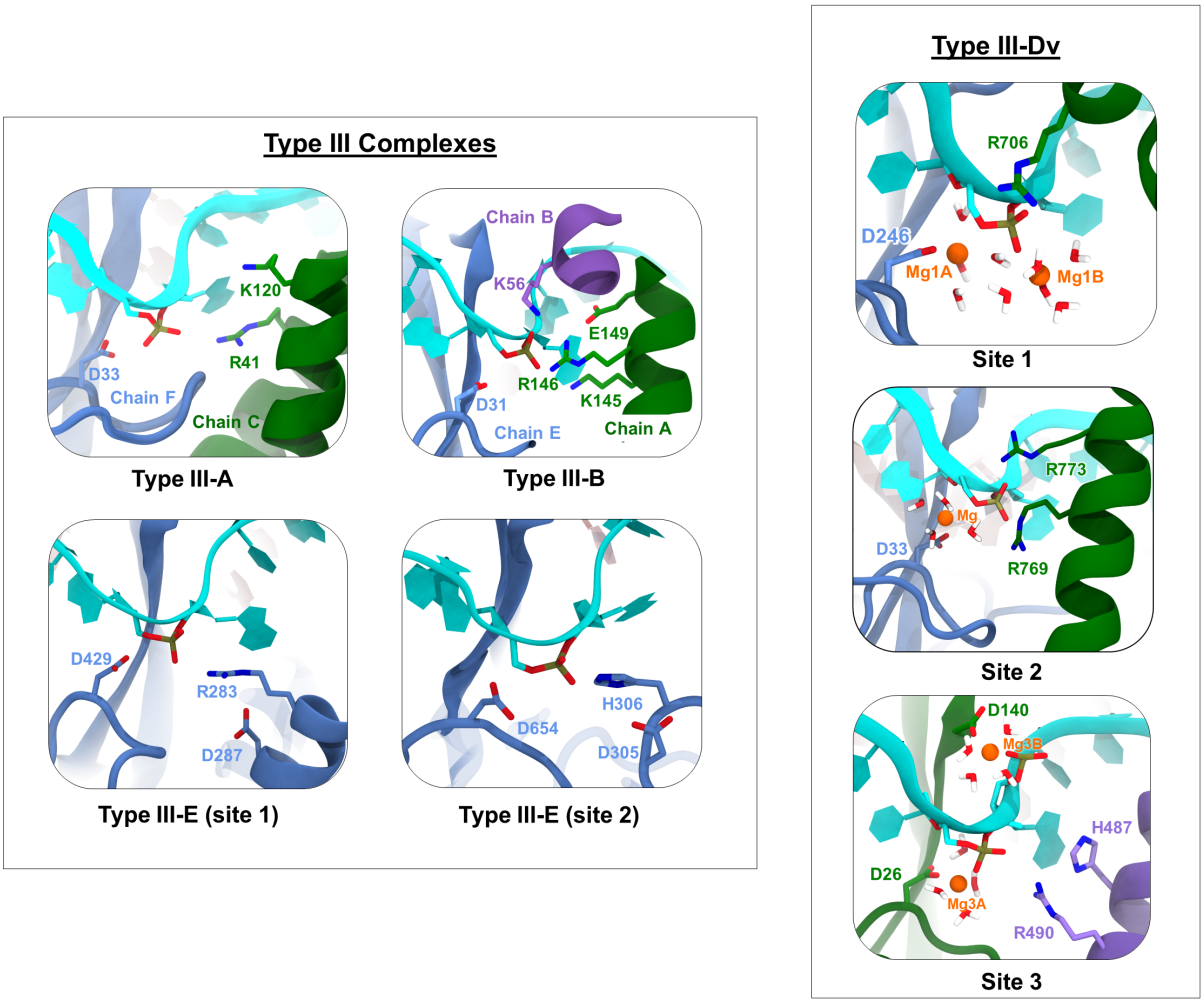

Ex. Data fig. 8 | Active site comparisons between the type III-Dv complex and other type III complexes. *Left*, Cas7 active sites from type III-A, -B and -E complexes. *Right,* Cas7 active sites from type III-Dv complex. The structural arrangement of active site 2 from the type III-Dv complex is similar to active sites from other type III complexes.